Study on dual peg-in-hole insertion using of constraints formed in the environment

Jianhua Su
Institute of Automation, Chinese Academy of Sciences, The State Key Laboratory of Management and Control for Complex Systems, Beijing, China
Rui Li
Institute of Automation, Chinese Academy of Sciences, The State Key Laboratory of Management and Control for Complex Systems, Beijing, China and University of the Chinese Academy of Sciences, Beijing, China
Hong Qiao
Institute of Automation, Chinese Academy of Sciences, The State Key Laboratory of Management and Control for Complex Systems, Beijing, China and Institute of Neuroscience, CAS Centre for Excellence in Brain Science and Intelligence Technology, Shanghai, China
Jing Xu
Lee Shau Kee Science and Technology Building, Tsinghua University, Beijing, China
Qinglin Ai
College of Mechanical Engineering, Zhejiang University of Technology, Beijing, China, and
Jiankang Zhu
Institute of Automation, Chinese Academy of Sciences, The State Key Laboratory of Management and Control for Complex Systems, Beijing, China

Abstract

Purpose – The purpose of this paper is to develop a dual peg-in-hole insertion strategy. Dual peg-in-hole insertion is the most common task in manufacturing. Most of the previous work develop the insertion strategy in a two- or three-dimensional space, in which they suppose the initial yaw angle is zero and only concern the roll and pitch angles. However, in some case, the yaw angle could not be ignored due to the pose uncertainty of the peg on the gripper. Therefore, there is a need to design the insertion strategy in a higher-dimensional configuration space.

Design/methodology/approach – In this paper, the authors handle the insertion problem by converting it into several sub-problems based on the attractive region formed by the constraints. The existence of the attractive region in the high-dimensional configuration space is first discussed. Then, the construction of the high-dimensional attractive region with its sub-attractive region in the low-dimensional space is proposed. Therefore, the robotic insertion strategy can be designed in the subspace to eliminate some uncertainties between the dual pegs and dual holes.

Findings – Dual peg-in-hole insertion is realized without using of force sensors. The proposed strategy is also used to demonstrate the precision dual peg-in-hole insertion, where the clearance between the dual-peg and dual-hole is about 0.02 mm.

Practical implications – The sensor-less insertion strategy will not increase the cost of the assembly system and also can be used in the dual peg-in-hole insertion.

Originality/value – The theoretical and experimental analyses for dual peg-in-hole insertion are proposed without using of force sensor.

Keywords Attractive region, Peg-in-hole, Sensor-less

Paper type Research paper

1. Introduction

Peg-in-hole insertion is a frequently performed automated mechanical assembly task. The objective of the task is to achieve the insertion from an unknown initial peg-in-hole configuration to a geometrical goal region under some constraints. It is generally believed that high-precision peg-in-hole insertion can only be achieved by a precision robot with the guidance of force sensors or by using flexible wrists.

1.1 Peg-in-hole insertion using force sensor

Obviously, the advantages of using force sensor are earlier contact detection and/or precisely force control, which will help

The current issue and full text archive of this journal is available on Emerald Insight at: **www.emeraldinsight.com/0143-991X.htm**

Industrial Robot: An International Journal
44/6 (2017) 730–740

[DOI 10.1108/IR-07-2016-0186]

This work is supported in part by NSFC-Zhejiang Joint Fund for the Integration of Industrialization and Informatization under Grant number U150921 and is supported by the Strategic Priority Research Program of the CAS (Grant XDB02080003).

Received 12 July 2016
Revised 12 April 2017
Accepted 14 April 2017

the robot to achieve high-precision peg-in-hole insertion when the inaccuracy of manipulator positioning exceeds assembly tolerances. In other words, with the aid of force sensory signals, it is possible to establish the mapping from the force/torque signals to the peg-in-hole configurations, as they enable us to design various force-feedback controllers for planning the robot's motion.

The need for force responsiveness in assembly has been recognized for more than 30 years. The studies of Inoue (1974) and Whitney (1982) have been recognized as important examples of force sensory feedback manipulations; since then, many sensor-based strategies have been developed. Skubic and Volz (2000) used force-based contact states to describe qualitatively how contact was being made with the environment. When a change occurs in qualitative, discrete state constitutes an event and triggers a new control command to the robot, which moves the assembly toward a new contact formation. Astuti and Mccarragher (1996) modeled the assembly process as a hybrid dynamic system consisting of a discrete event system and a continuous time system, and then proposed a discrete event controller (DEC) synthesis methodology resulting in convergence in a minimum number of events. Newman *et al.* (1999) addressed the problem of force-responsive automated assembly which includes contact stability, the force responsiveness, etc. In their work, the robot was controlled to be responsive to the forces and accelerations and capable of regulating its endpoint dynamics on demand. De Schutter *et al.* (1987) realized a peg-in-hole insertion with active force feedback involving fragile and medium-sized workpieces; in the assembly, the interaction forces were used to modify or even generate the desired trajectory of the robot. Huang and Schimmels (2004) addressed the design of the appropriate admittance matrix for force assembly of a polyhedral rigid body. They identified the conditions that restricted the admittance behavior for each of the various one-point and two-point contact cases and ensured that the motion reduced part misalignment. Lange *et al.* (2010) used feed-forward controller to improve the accuracy of the assembly and also ensured the fastest possible response to external disturbances. Their method was applied to assembly wheels to a car body. Shirinzadeh *et al.* (2011) presented a robot-based height adjustment method for the assembly of cylindrical pairs. In their work, the peg-in-hole strategy was used by decreasing the contact forces between the manipulator and the fixture. Lefebvre *et al.* (2005) developed a Bayesian estimator to estimate the position and orientation inaccuracies of contacting objects during force-controlled compliant motion, in which the estimation is based on position, velocity and force measurements. Robuffo Giordano *et al.* (2008) computed a setup and robot motion that maximizes regions of attraction in which the robot was impedance controlled, using internal torque sensors instead of a wrist force sensor. Sathirakul and Sturges (1998) enumerated possible contact states of dual peg-in-hole insertion, and derived geometric conditions and force-moment equations for static-equilibrium states of dual peg insertion. Thus, they obtained the taxonomy of dual-peg insertions. Fei and Zhao (2005) analyzed the assembly contact and geometric conditions of a dual peg-in-hole in three dimensions. With the static equilibrium equations, the relationship between forces and moments for maintaining each contact state was derived.

However, there are also some limits to the application of the force sensor in manufacturing. For example:

- a sensor system increases the initial cost to the system;
- a sensor reduces the robustness and reliability of the whole system; and
- moreover, in certain cases, the states measured by sensors may be different from that ground truth (Qiao and Zhang, 2000).

Due to the high cost and maintenance difficulty of high-precision sensors, many tedious works still need to be done manually or with low-precision sensors. Therefore, research on low-precision systems that use few sensors or even no sensors to achieve high-precision tasks are very important for manufacturing.

1.2 Peg-in-hole insertion without force-sensor

On the other hand, manipulation without force-sensor has been investigated for many years. Some works focus on eliminating the uncertainty of the system based on limited sensor information. The purpose of insertion without force-sensor is to find a region from which a peg can be guided to the goal by using a unique input based on the constraints of the environment rather than by using force sensor.

Lozano-Pérez *et al.* (1984) outlined a pre-image approach to directly incorporate the effect of uncertainty within the planning process. The pre-image approach first computes the pre-image of a goal, then recursively backchains and computes the pre-image of the pre-image, and so forth. In this fashion, the planner determines a chain of pre-images specifying a sequence of motion commands guaranteed to reach the goal. Erdmann (Erdmann, 1986; Erdmann and Mason, 1988) formed the fundamental theory of back-projection approach and applied to peg-in-hole strategy. The back-projection of a desired goal consists of all those points that are guaranteed to reach the goal. In addition, all points from which a trajectory could reach an undesirable point were also marked as undesirable. Chen *et al.* (2009) applied a soft servo strategy to achieve the tight-tolerance assembly with the compliance of the robot and the environment, that is, industrial robots can be made compliant to the environment when the control loop gains are reduced, which is a so-called soft servo capability. Balkcom *et al.* (2002) derived an algorithm that determined the external wrenches consistent with constraints on the contact interactions between two rigid planar bodies, and then used it to create sensorless plans that guaranteed that a workpiece was correctly inserted into a fixture. Robertsson *et al.* (2012) presented a method of doing force control without a force sensor in which the motor current was evaluated to detect when a phase of the assembly strategy had been completed. Polverini *et al.* (2016) proposed an active compliance admittance-based method combined with trajectory generation to perform the insertion task, in which the trajectory generator is merged together with robot position/velocity controller. Their method relies on the model-based sensor-less observer of interaction forces and is no need of external force sensor. Matsuno *et al.* (2004) inserted a long peg into a tandem shallow hole using search trajectory generation without force feedback. In their insertion system, the input is the desired position of a gripping point. A manipulator recognized the availability of insertion operation, and if the

insertion operation is available, the manipulator continued the task keeping a trajectory; otherwise, the manipulator searches the correct posture of the peg.

Manipulation without force-sensor should bring some benefits:

- it deduces the initial cost of the assembly system; and
- it can avoid effect of sensor noise on the accuracy of the insertion.

However, there are also some difficulties in assembly without force sensor, such as how to make sure that the planned path is exactly compliant to the desired contact state, especially when the configuration space of such a contact state is hard to describe analytically due to high dimensionality. Most of the previous peg-in-hole insertion methods are outlined in a two- or three-dimension configuration space, where some degrees of freedom of the peg are ignored.

1.3 The purpose of this work

Dual peg-in-hole insertion is a common task in the industry assembly task such as the assembly of reducers, engine cylinder, etc. Most of the previous work analyzed the insertion in a two- or three-dimension space, in which they suppose the initial yaw angle is zero and only concern only roll angles. However, in some cases, both roll and pitch rotations could be taken into account due to the position uncertainty of the peg on the gripper. Therefore, we need to design the insertion strategy in a higher dimensional configuration space.

In our previous work (Qiao *et al.*, 2015), we formed a constraint region in an environment to eliminate the uncertainty of the system and achieve single peg-in-hole insertion; we called this region as the "attractive region in environment". In this paper, we aim to push the attractive region method to dual peg-in-hole insertion, and consequently, some theorems, to judge the existence of the attractive region in dual peg-in-hole insertion, are proposed.

To the best of our knowledge, there is few work that discuss the sensor-less dual peg-in-hole insertion. To deal with the problem, the major contributions of this paper are as follows:

- a sensor-less dual peg-in-hole insertion strategy is developed based on the attractive region formed by the constraints;
- the proposed method is applied to the assembly of two eccentric shafts of a reducer into the supporting flange; and
- the decomposition of the high-dimension attractive region into its sub-attractive region in the low-dimension space is presented.

The rest of the paper is organized as follows. Section 2 discusses the construction of the attractive region formed in the configuration space of assembly system. In Section 3, we decompose the high-dimensional configuration space into several low-dimensional ones and then design the insertion strategy based on the sub-space. In Section 4, an example of dual peg-in-hole insertion is presented to explain the proposed method, and two experiments are conducted to illustrate the proposed method. Section 5 concludes the paper.

2. Analysis of the dual peg-in-hole insertion

2.1 Definition of the attractive region

Assume that there is a non-linear system:

$$\dot{X}(t) = f(X(t), u(t)) \tag{1}$$

where $X(t) \in U \subset \mathrm{R}^n$ is the state vector, $u(t) \in V \subset \mathrm{R}^m$ is the input vector and $f : U \times V \mapsto \mathrm{R}^n$ is a function defined in arbitrary subsets of the n-dimensional real number set R^n.

For all, $X(t) \in \Omega \subset U$, if there exists a special function $g : \Omega \mapsto \mathrm{R}^1$ satisfying the following properties:

- *C1*. $g(X) = g(X_0)$ when $X = X_0$, $g(X) > g(X_0)$ when $X \in \{U - X_0\}$;
- *C2*. $g(X)$ has continuous partial derivatives with respect to all the components of X; and
- *C3*. $\mathrm{d}g(X)/\mathrm{d}t < 0$ where $X \in \{U - X_0\}$.

Then, the system is stable in the region Ω, which is called the "attractive region" (Qiao *et al.*, 2015). The special function $g(X)$ is the attractive function.

It should be noted that the input vector $u(t)$ is a state-independent input. We now explain the concept of an "attractive region" by using a dynamical system. Let us consider the example of a bean and bowl from the viewpoint of a dynamical system. As illustrated in Figure 1, if the goal is to make the bean reach the bottom of the bowl, then no matter where the initial position of the bean is, with gravity, it would eventually reach the bottom of the bowl. In this case, the position of the bean can be treated as the state of a system, and the bowl as some constraints formed by the environment. Under the effect of gravity, which is a state-independent input to the system, the state would finally converge to the goal region. In this process, it should be noted that the size of the goal region is smaller than that of the initial region; that is, the uncertainty of the system is eliminated.

2.2 Construction of the attractive function

Here, we discuss the construction of the attractive function for dual peg-in-hole insertion.

To develop strategies for robotic dual peg-in-hole insertion, it is useful to analyze the total allowable range of the pegs considering the constraints from the holes. For simplicity, we use the direction cosines of the axes of the two pegs, i.e. the cosines of the angles between the z_{p}-axis and the three coordinate axes of the H-frame, to represent the orientation of the dual pegs. It should be noted that we usually use Euler angles to represent the robot's end-effector orientation. It should also be noted that we can also transform the Euler

Figure 1 Example of an attractive region in the motion region of a bean under the constraints of a bowl

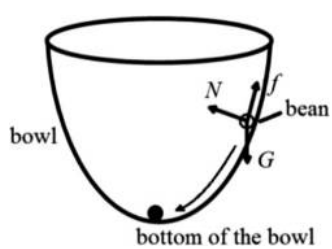

angles to the direction cosines of the pegs. The lowest point of the peg is usually the point on the end surface of the peg that has the minimum z_{pl} in the H-frame, as shown in Figure 2.

- The H coordinate frame is fixed to the plane passing through the upper surface of the two holes; O_h is defined as the center of the line passing through the centers of the two holes on the upper surface, O_hY_h is defined as the line passing through the centers of the two holes, O_hZ_h is the line along the axis of the hole in the upward direction, and O_hX_h is the line perpendicular to O_hY_h and O_hZ_h.
- The P coordinate frame is fixed to the plane passing through the end surface of the two pegs; O_p is defined as the center of the end surface of the two pegs, O_pY_p is the line parallel to the projection of O_hY_h on the end surface of the two pegs, O_pZ_p is the line along the axis of the peg in the upward direction, and O_pX_p is the line perpendicular to O_pY_p and O_pZ_p.

The pose of the dual pegs in the H-frame is described by $(x_p, y_p, z_p, \theta_{px}, \theta_{py}, \theta_{pz})$, where x_p, y_p, z_p represent the position of O_p on the H-frame, and $(\theta_{px}, \theta_{py}, \theta_{pz})$ are the angles between the axis of the dual pegs, i.e. z_p-axis, and the three coordinate axes of the H-frame. The computation of the contact points between the dual-peg and the dual-hole is described in Appendix.

Figure 3 describes several contact states between the dual-peg and dual-hole. Figure 3(a) shows a one-point contact state in which the side surface achieves contact between the right peg and the right hole. Figure 3(b) shows a two-point contact state in which the projection shows the state that the bottom surface of the right peg is in contact with the right hole, and the lowest point of the right peg is inside the right hole. Figure 3(c) shows a three-point contact. The projection shows the state in which the bottom surface of the right peg is in contact with the right hole, and the lowest point of the right peg is inside the right hole. Figure 4(d) shows a six-point contact. The projection shows the state in which the bottom surfaces of the pegs are in contact with the holes, and the lowest point of the right peg is inside the right hole. In Figure 3(b)-(d), the blue solid lines denote the hole, and the red dot lines denote the projection of the pegs. The contact points are marked with a black dot.

Once the contact points are obtained, we can establish a deterministic function of the height of O_p, i.e. z, respect to the pose $(x_p, y_p, \theta_{px}, \theta_{py}, \theta_{pz})$, which is an attractive function in a six-dimensional configuration space, as expressed follows:

$$z = g(x_p, y_p, \theta_{px}, \theta_{py}, \theta_{pz}) \tag{2}$$

However, the design of robotic manipulation in very high-dimensional spaces is obviously quite difficult. In general, converting the higher-dimensional problems into a set of lower-dimensional ones can be used to solve the problem. In this work, the seven-dimensional space is converted into several subspaces; hence, dual peg-in-hole insertion can be designed in these low-dimensional configuration spaces.

Figure 2 Coordinate frame used in the dual peg-in-hole insertion system

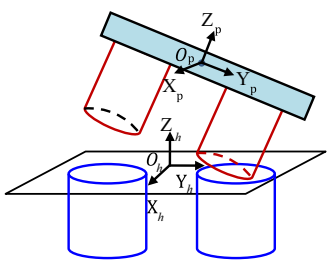

Figure 3 Example of the contacts between the pegs and the holes in which the black points denote the contact points

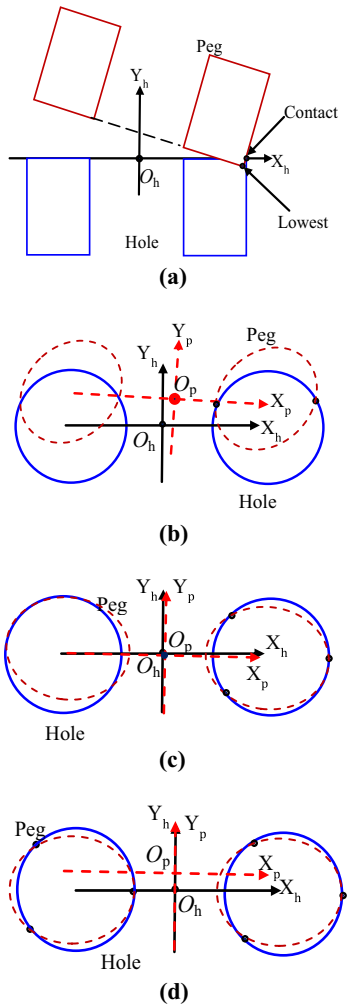

Notes: (a) One-point contact; (b) two-point contact; (c) three -point contact; (d) six-point contact

3. Dual peg-in-hole insertion

In this section, we convert the six-dimensional configuration space into a set of subspaces. Then, we can build the sub attractive functions and design the dual peg-in-hole insertion. We assume that the function $g(x_p, y_p, \theta_{px}, \theta_{py}, \theta_{pz})$ be a smooth function with continuous first- and second-order partial derivatives with respect to all components. Thus, we can get the following sub attractive functions as follows.

3.1 Sub attractive function $g_{1,i}$

In equation (2), we set $(\theta_{px}, \theta_{py}, \theta_{pz}) = (\theta^i_{px}, \theta^i_{py}, \theta^i_{pz})$ that are some fixed angles. Denote the sub function $g_{1,i}$ by:

Figure 4 (a) The graph of the attractive region that the dual-peg moves along x_h and y_h-axis with fixed (θ^i_{px}, θ^i_{py}, θ^i_{pz}); (b) corresponds to State 1; (c) corresponds to State 2; (d) relates to the configuration on arrival at the bottom of the attractive region

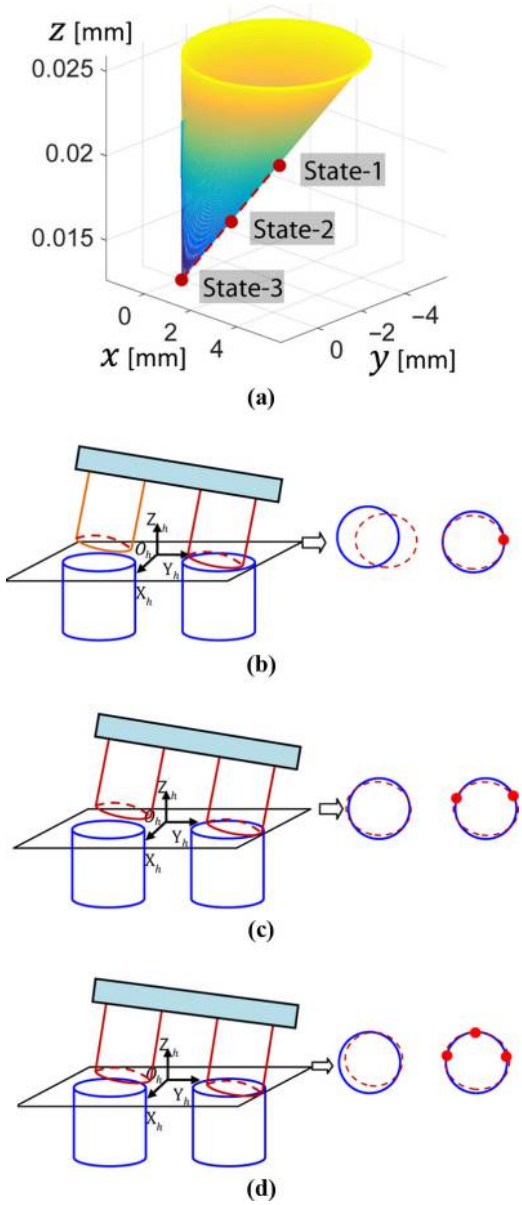

$$g_{1,i} = g\left(x_p, y_p, \theta_{px}, \theta_{py}, \theta_{pz}\right)\big|_{\theta_{px},\theta_{py},\theta_{pz}=\theta^i_{px},\theta^i_{py},\theta^i_{pz}} \tag{3}$$

Under fixed (θ^i_{px},θ^i_{py},θ^i_{pz}), three contact configurations possibly exist between the pegs and the holes when we adjust the pose of the dual peg-in-hole:

- Neither of the two pegs have contact points with the two holes.
- The left peg has no contact point with the left hole, but the right peg has contact points with the left hole.
- Both the pegs have contact points with the two holes.

As an example, we set $\theta_{px}=\pi/3$, $\theta_{py}=0$, $\theta_{pz}=0$. Thus, when contact points exist between the left peg and the left hole, we can obtain the following equations:

$$(x_p + x_0 - 1)^2 + (0.5y_p + y)^2 = 6 \tag{4}$$

$$x_p + \sqrt{3}y_p/2 + 0.5z_p + z = 0 \tag{5}$$

$$(x_p - 1)^2 + {y_p}^2 = 6 \tag{6}$$

$$z_p \in [0, h] \tag{7}$$

From equations (4)-(7), we can established a deterministic function of the height of O_p, i.e. z, respect to the translation along x_h- and y_h-axis, i.e. (x,y). An example of the graph of the function is shown in Figure 4, which also presents the analysis of the relations between the configuration in the attractive region and the physical contact state of the dual pegs and dual holes. The three states, i.e. State-1, State-2 and State-3, describe three contact states between the dual-peg and the dual-hole.

The steps to eliminate the uncertainties of the dual pegs along the x_h-, y_h- directions are as follows. In State-1 and State-2, the right peg has one or two contact points with the right hole; this is related to the configuration near the bottom of the attractive region. In State-3, the right peg has three contact points with the right hole; this is related to the configuration on arrival at the bottom of the attractive region. In this case, the uncertainties of the right peg along the x_h-, y_h- directions are eliminated by the constraints of the right hole. In other words, $g_{1,i}$ reaches its minimum.

Figure 4(a) shows the graph of the attractive region that the dual-peg moves along x_h and y_h-axis with fixed (θ^i_{px}, θ^i_{py}, θ^i_{pz}); Figure 4(b) reports that the right peg has one contact points with the right hole, which corresponds to State 1; Figure 4(c) reports that the right peg has two contact points with the right hole when we move it along -y_h direction, which corresponds to State 2; Figure 4(d) reports that the right peg has three contact points with the right hole when we move it along -x_h direction; this is related to the configuration on arrival at the bottom of the attractive region. In Figure 4(b)-(d), the left show the projection of the dual-peg on the hole in which the blue solid lines denote the hole and the red dot lines denote the projection of the pegs. The contact points are marked with red dot.

The minimum of sub-function $g_{1,i}$ means that, under fixed orientation (θ^i_{px},θ^i_{py},θ^i_{pz}), the motion of the peg along x_h- and y_h-axes are constrained by the hole. It should be noted that the peg is able to move along x_h- and y_h-axes again if its orientations (θ_{px},θ_{py},θ_{pz}) are changed. In this case, we should continuously push the new sub-function $g_{1,i+1}$ to reach to its minimum, as illustrated in the following step.

3.2 Sub-attractive function $g_{2,j}$

Sub-function $g_{2,j}$ is defined as:

$$g_{g_{2,j}}\left(\theta_{px}, \theta_{py}\right) = \left\{ \min_{\theta^i_{px},\theta^i_{py}} g_{1,i} \right\} \tag{8}$$

Figure 5 shows the graph related to equation (8). Each configuration in the attractive region is determined by the minimum of sub-function $g_{1,i}$ under different angles θ_{px}, θ_{py}.

Figure 5 (a) The graph of the attractive region with changing θ_{px} and θ_{py}. (b) shows three contact points; (c) shows four contact points; and (d) shows there are six contact points

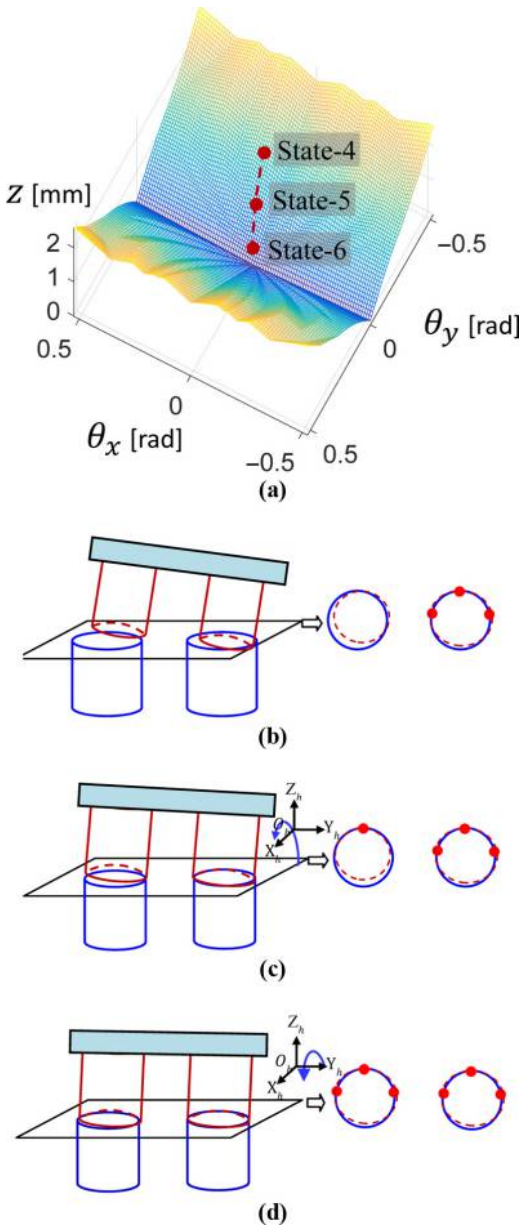

The steps to eliminate the uncertainties of the dual pegs related to the dual holes are as follows. In State-4, the two pegs have three contact points with the two holes: the right peg and right hole have three contact points, and the left peg and right hole have no contact point. To achieve four contact points shown in Figure 5(c), we need to adjust angles (θ_{px}, θ_{py}). At the new orientation, we can make $g_{2,j}$ approach to State-5, which is related to a six-point contact-state, as shown in Figure 5(d). In this case, the right peg has three contact points with the right hole, and the left peg has three contact points with the left hole. Figure 5(a) shows the graph of the attractive region with changing θ_{px} and θ_{py}. Figure 5(b) shows that the right peg and right hole have three contact points, and the left peg and right hole have no contact point. Notice that Figure 5(b) corresponds to State-4 of the attractive region. Figure 5(c) shows that the right peg and right hole have three contact points, and the left peg and right hole have one contact point when we rotate the dual-peg around x_h-axis. Notice that Figure 5(c) corresponds to State-5 of the attractive region. Figure 6(d) shows that the right peg and right hole have three contact points, and the left peg and right hole have three contact point when we rotate the dual-peg around y_h-axis. Notice that Figure 5(d) corresponds to State-6 of the attractive region.

The minimum of sub-function $g_{2,j}$ means that, under fixed orientation θ^j_{pz}, the rotation of the peg around x_h- and y_h- axes are constrained by the hole.

3.3 Sub-attractive function g_3

Sub-function g_3 is defined as:

$$g_3(\theta_{pz}) = \left\{ \min_{\theta^j_{pz}} g_{2,j} \right\} \tag{9}$$

An example of the graph of g_3 is shown in Figure 6. Each configuration on the curve is determined by the minimum of sub-function $g_{2,j}$ under different angles θ_{pz}. The bottom of the curve represents the minimum of g_3, which implies that the motions of the peg along x_h-, y_h-axes, and the rotations around x_h-, y_h-axis

Figure 6 (a) The graph of the attractive region with changing θ_{pz}; (b) shows that both the right peg-in-hole and the left peg-in-hole have three contact points, which corresponds to State-7; and (c) shows that the dual-peg has been inserted into the dual-hole, which corresponds to State-8 of the attractive region

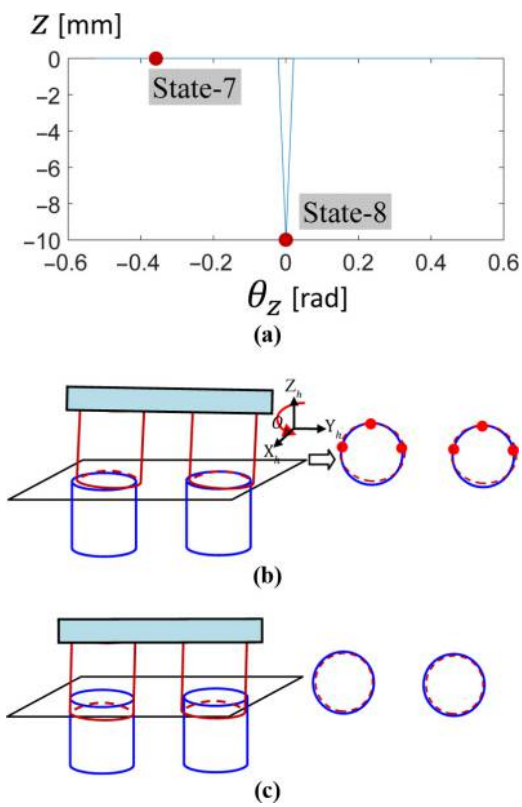

are constrained by the hole. Finally, g_3 reaches its minimum, which corresponds to the state in which the dual pegs have been inserted into the dual holes, as shown in Figure 6(d).

3.4 Computational complexity

The construction of the attractive regions generally needs to traverse all the possible state of the dual peg in the configuration space. Thus, the time complexity of the proposed algorithm is of $O(N^2+N^2+N^1)$ for a five-dimensional input data, while direct calculation of attractive region has a complexity of $O(N^5)$.

To illustrate the proposed strategy and show the efficiency of the dual peg-in-hole insertion, experiments on the assembly of a typical dual peg-in-hole with 0.02 mm clearance, and the assembly of a cycloid reducer are presented in the next section.

4. Experiments

To validate our approach, we have implemented two peg-in-hole insertion tasks. Experiment 1 shows a typical dual peg-in-hole insertion in which the radius of the peg is about 19.98 mm while that of the hole is 20.00 mm with a clearance about 20 μm. Experiment 2 describes that two eccentric shafts in the reducer are inserted into the two holes in the supporting flange. The lower circle radius of the conical eccentric shaft is about 24.96 mm while that of the hole in the supporting flange is 25.00 mm with a clearance about 40 μm.

4.1 Experiment on dual peg-in-hole

This experiment is performed by a 6-DoFs YASKAWA robot with position repeatability of 0.06 mm. A force/torque sensor is mounted on the end-effector of the robot to record the inserting force. It should be noted that the force signal is not used for control but only used to record the inserting force. The radius of the peg is about 19.98 mm while that of the hole is 20.00 mm with a clearance about 20 μm. With such a small clearance, it is hard to insert the peg directly using of the position control method.

We repeat the insertion experiment 30 times with the proposed sensor-less assembly method, in which we get 100 per cent success rate. In Figure 7, the inserting process is briefly described follows:

Remark: It should be noted that, it is hard to achieve the assembly of 0.02 mm clearance parts by the robot with position repeatability of 0.06 mm only using of position feedback. Two errors will prevent the insertion:

1. the error between the actual goal pose and the ideal goal pose of the dual-hole; and
2. the motion error of the robot end-effector.

The "attractive region" formed by the dual-hole could be used to eliminate the pose uncertainties of the dual-peg related to the dual-hole. In other word, we do not need the dual-peg arrive to a precision goal position but only need to arrive to the "mouth" of the region.

In the experiment shown in Figure 8, we set soft floating function on 4, 5 and 6 axis, and then rotate the dual-peg around x_h- y_h- and z_h-axis meanwhile move along z_h-axis. Thus, the constraints of the dual-hole would lead the dual-peg transfer from the surface of the attractive region to its minimum, as described in Figures 4(a), 5(a) and 6(a).

In the following, we compare the proposed method with force-guided method. We measure the contact forces and torques of the end-effector in inserting as shown in Figures 9 and 10.

Figure 9 shows results of the time evolution of the obtained contact force vector components (*Fx*, *Fy*, *Fz*, *Mx*, *My*, *Mz*) of the robot using of the sensor-less method. It can be observed that *Fx*, F*y* and *Fz* exhibit steps, which indicate occurrences of contact between the peg and the receptive part. The whole inserting time is about 6 s.

Figure 10 shows results of the time evolution of the obtained contact force vector components (*Fx*, *Fy*, *Fz*, *Mx*, *My*, *Mz*) of the robot using of the force-guided method. The whole inserting time is about 100 s.

Notice that Fei and Zhao (2005) assume that the rotation angle of the dual-peg around the axis of the dual-peg is zero, i.e. $\theta_z = 0$; thus, the analysis of the insertion is in a three-dimensional configuration space. In their experiment, the clearance between the dual-peg and dual-hole is about 0.1 mm, where the radius of the hole is 10 mm and the radius of the peg is 9.9 mm. The maximum of the inserting force is about 200 N.

In this work, we take the uncertainties of θ_z into account; thus, the analysis of the insertion is in a six-dimensional configuration space. In our experiment, the clearance between the dual-peg and dual-hole is about 0.02 mm, where the radius of the hole is 20 mm and the radius of the peg is 19.98 mm. The maximum of the inserting force is about 100 N and the inserting time is about 6 s. The major advantage of our method is the low-cost of the assembly system without using of force sensors.

Figure 7 The insertion steps

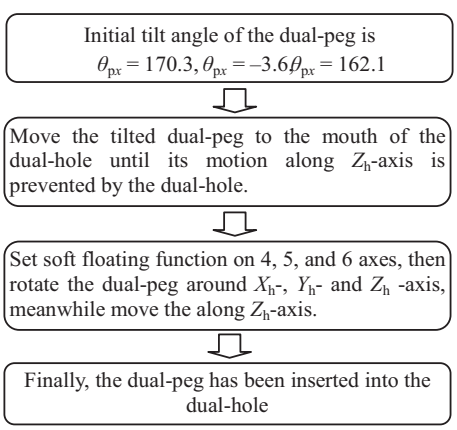

4.2 Experiment on assembly of the cycloid reducer

Manufacturing of reducers, which are widely used in robotics systems, is an important task in the robot manufacturing industry. Each reducer is assembled from thirty components in which the dual peg-in-hole insertion is an important and difficult task in the assembly. As shown in Figure 11, there are two eccentric shafts in the reducer, which need to be inserted into the two holes in the supporting flange. The max radius of the cone roller is about 24.96 mm while that of the hole in the supporting flange is 25.00 mm with a clearance about 40 μm.

Our experiments are performed by a 6-DoFs robot of Googol Technology Ltd., which is equipped with a four-pin pneumatic

Figure 8 Insertion of the dual-peg into the dual-hole

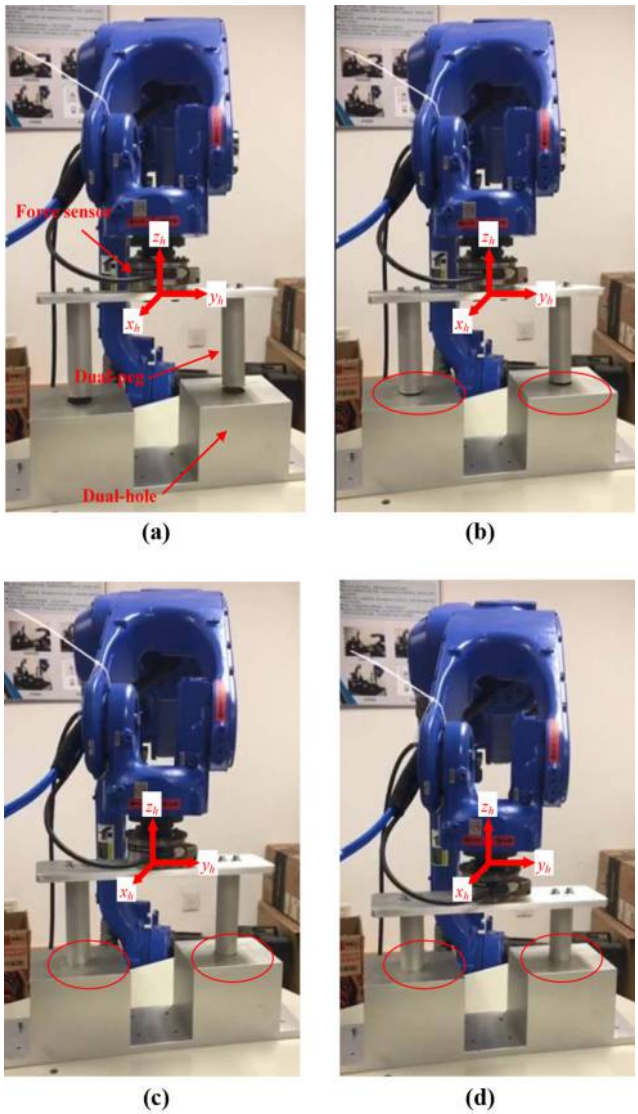

Notes: (a) Shows that the tilt dual-peg approach to dual-hole; (b) shows that we rotate the dual-peg around x_h-, y_h- and z_h-axis meanwhile move along zh-axis; (c) shows that we set float and then rotate and move the dual-peg; and (d) shows that the dual-hole has been inserted into the dual-peg

Figure 9 The force/torque in inserting using sensor-less method

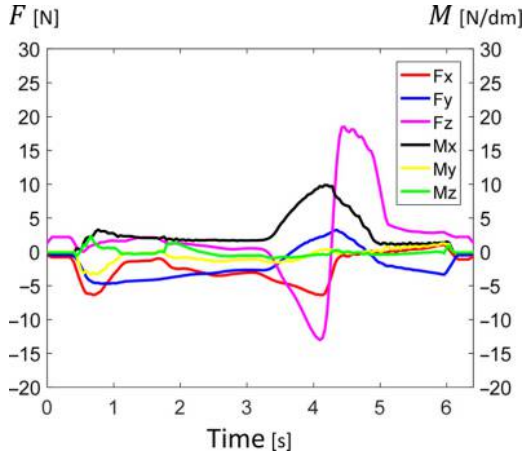

Figure 10 The force/torque in inserting using force-guided method

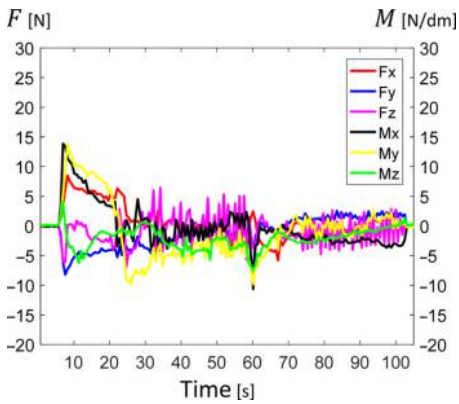

Figure 11 A case of dual peg-in-hole insertion

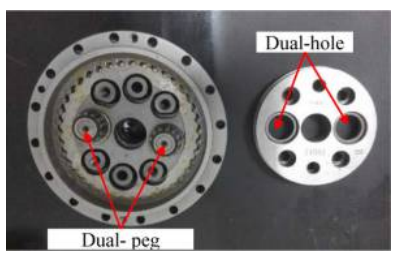

gripper. The pose error of the supporting flange on the gripper is larger than 1 mm. Thus, it is difficult to realize the dual peg-in-hole insertion (the precision is less than 1 mm) by relying only on the precision of the robot itself.

Initially, as shown in Figure 12(a), we fix the orientation of the dual-hole, and then move it along the x_h, y_h and z_h directions until its motion along z_h axis is prevented by the dual-peg.

Next, as shown in Figure 12(b), we decrease the angles (θ_{px}, θ_{py}) meanwhile move the robot end-effector along z_h direction until the motion is prevented by the dual-peg. In this case, we achieve a six-point contact state, which means that the translation uncertainties along the x_h and y_h-directions and the rotation uncertainties around the z_h-axis are eliminated by the constraints of the dual-hole.

Then, as shown in Figure 12(c), we rotate the angle θ_{pz}, meanwhile move the dual-hole along Z_h-directions until the dual-hole are fully inserted into the dual-peg, that is, all the uncertainties of the dual-hole and dual-peg are eliminated by the constraints of the dual-peg.

In this work, we provide a solution to deal with the high-dimensional insertion problem by converting it into several

Figure 12 Insertion of the two eccentric shafts and the supporting flange

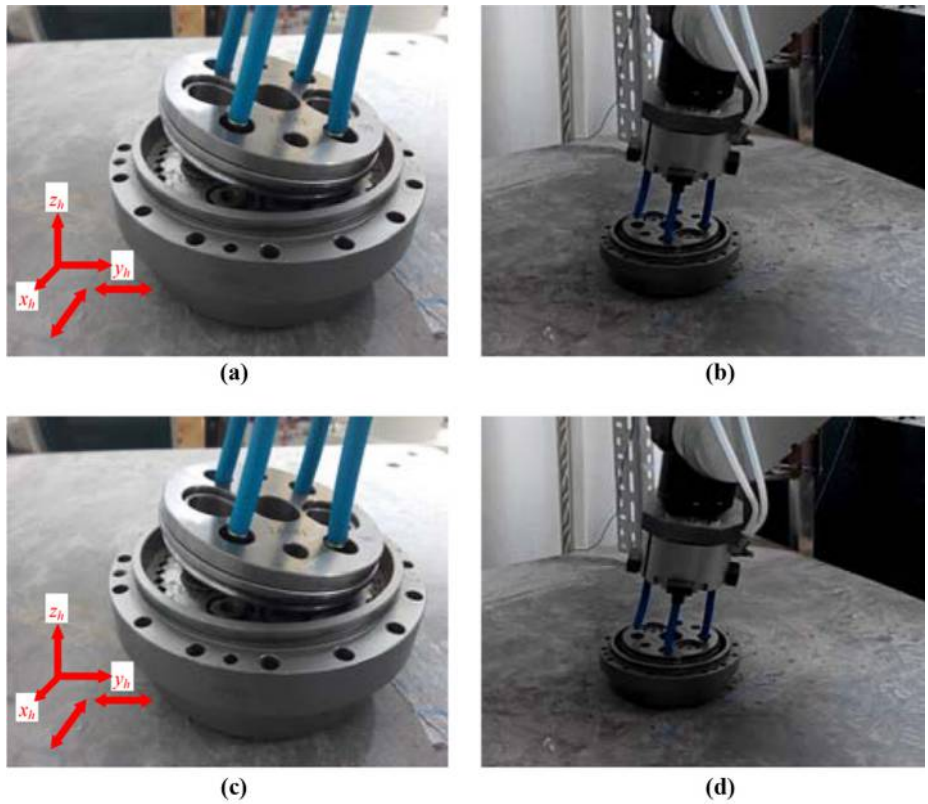

Notes: (a) Shows that we fix (θ_{px}, θ_{py}, θ_{pz}) but let the dual-hole to follow a nominal trajectory; (b) shows that we decrease the angles (θ_{px}, θ_{py}) but fixed the angle θ_{pz}; (c) shows that we decrease the angle θ_{pz}; and (d) shows that the dual-hole is been fully inserted into the dual-peg

subproblems. We present a decomposing method to convert the high-dimensional configuration space into a set of subspaces. In each subspace, robotic manipulation is designed to eliminate some uncertainties between the pegs and the holes. Hence, we can find manipulation in a low-dimensional configuration space that would achieve dual peg-in-hole insertion. The proposed strategy is used to demonstrate the precision assembly of dual-peg and dual-hole. We also perform two experiments to show the efficiency of the strategy.

The advantage of the sensor-less assembly method is that we achieve high-precision tasks without force sensors, as that would deduce the initial cost of the assembly system and can avoid effect of sensor noise on the accuracy of the assembly.

However, the decomposition method requires the shape of the initial space should be a convex shape. For example, we can deal with the cylinder peg-in-hole with the method due to the attractive region formed in the insertion of cylinder peg is a convex shape. It is difficult to design the insertion strategy based on the decomposition method for irregular peg, as the attractive region formed in the insertion of irregular peg is usually a non-convex shape.

In the future work, we will give the conditions of which shape attractive region can be decomposed.

References

Astuti, P. and Mccarragher, B.J. (1996), "Discrete event controller synthesis for the convergence of an assembly process", *IEEE International Conference on Robotics and Automation*, *Minneapolis*, *MN*, 22-28 April, pp. 1153-1158.

Balkcom, D.J., Gottlieb, E.J. and Trinkle, J.C. (2002), "A sensorless insertion strategy for rigid planar parts", *IEEE International Conference on Robotics and Automation*, *Washington DC*, 12-18 May, pp. 882-887.

Chen, H.P., Wang, J.J., Zhang, G., Fuhlbrigge, T. and Kock, S. (2009), "High-precision assembly automation based on robot compliance", *International Journal of Advanced Manufacturing Technology*, Vol. 45, pp. 999-1006.

De Schutter, J., Katupitiya, J., Vanherck, P. and Brussel, H.K. (1987), "Active force feedback in industrial robotic assembly: a case study", *International Journal of Advanced Manufacturing Technology*, Vol. 2, pp. 27-40.

Erdmann, M.A. (1986), "Using back-projections for fine motion planning with uncertainty", *The International Journal of Robotics Research*, Vol. 5 No. 1, pp. 19-45.

Erdmann, M.A. and Mason, M.T. (1988), "An exploration of sensorless manipulation", *Journal of Robotics and Automation*, Vol. 4 No. 4, pp. 369-379.

Fei, Y.Q. and Zhao, X.F. (2005), "Jamming analyses for dual peg-in-hole insertions in three dimensions", *Robotica*, Vol. 23 No. 1, pp. 83-91.

Huang, S. and Schimmels, J.M. (2004), "Admittance selection for force-guided assembly of polygonal parts despite friction", *IEEE Transactions on Robotics*, Vol. 20 No. 5, pp. 817-829.

Inoue, H. (1974), *Force Feedback in Precise Assembly Tasks*, AIM 308 Artificial Intelligence Lab MIT.

Lange, F., Scharrer, J. and Hirzinger, G. (2010), "Classification and prediction for accurate sensor-based assembly to moving objects", *IEEE International Conference on Robotics and Automation, Anchorage, AK*, 3-7 May, pp. 2163-2168.

Lefebvre, T., Bruyninckx, H. and Schutter, D.J. (2005), "Polyhedral contact formation identification for autonomous compliant motion: exact nonlinear bayesian filtering", *IEEE Transactions on Robotics*, Vol. 21 No. 1, pp. 124-129.

Lozano-Pérez, T., Mason, M.T. and Taylor, R.H. (1984), "Automatic synthesis of fine-motion strategies for robots", *The International Journal of Robotics Research*, Vol. 3 No. 1, pp. 3-24.

Matsuno, T., Fukuda, T. and Hasegawa, Y. (2004), "Insertion of long peg into tandem shallow hole using search trajectory generation without force feedback", *IEEE International Conference on Robotics and Automation, New Orleans, LA*, 26 April-1 May, pp. 1123-1128.

Newman, W.S., Branicky, M.S., Podgurski, H.A., Chhatpar, S., Huang, L., Swaminathan, J. and Zhang, H. (1999), "Force-responsive robotic assembly of transmission components", *IEEE International Conference on Robotics and Automation, Detroit, MI*, 10-15 May, Vol. 3 pp. 2096-2102.

Polverini, M.P., Zanchettin, A.M., Castello, S. and Rocco, P. (2016), "Sensorless and constraint based peg-in-hole task execution with a dual-arm robot", *IEEE International Conference on Robotics and Automation, Stockholm*, 16-21 May, pp. 415-420.

Qiao, H., Wang, M., Su, J.H., Jia, S.X. and Li, R. (2015), "The concept of 'attractive region in environment' and its application in high-precision tasks with low-precision systems", *IEEE Transactions on Mechatronics*, Vol. 20 No. 5, pp. 2311-2327.

Qiao, H. and Zhang, B. (2000), "Combination of strategy investigation and utilization of sensor signals in robotic assembly", *Journal of Engineering Manufacture*, Vol. 214, pp. 657-669.

Robertsson, A., Stolt, A., Linderoth, M. and Johansson, R. (2012), "Force controlled robotic assembly without a force sensor", *IEEE International Conference on Robotics and Automation, Saint Paul, MN*, 14-18 May, pp. 1538-1543.

Robuffo Giordano, P., Stemmer, A., Arbter, K. and Albu-schäffer, A. (2008), "Robotic assembly of complex planar parts: an experimental evaluation", *IEEE/RSJ International Conference on Intelligent Robots and Systems, Nice*, 22-26 September, pp. 3775-3782.

Sathirakul, K. and Sturges, R.H. (1998), "Jamming conditions for multiple peg-in-hole assemblies", *Robotica*, Vol. 16, pp. 329-345.

Shirinzadeh, B., Zhong, Y., Tilakaratna, P.D.W., Tian, Y. and Dalvand, M.M. (2011), "A hybrid contact state analysis methodology for robotic-based adjustment of cylindrical pair", *International Journal of Advanced Manufacturing Technology*, Vol. 52 No. 4, pp. 329-342.

Skubic, M. and Volz, R.A. (2000), "Acquiring robust, force-based assembly skills from human demonstration", *IEEE Transactions on Robotics and Automation*, Vol. 16 No. 6, pp. 772-781.

Whitney, D.E. (1982), "Quasi-static assembly of compliantly supported rigid parts", *Transactions on ASME Journal of Dynamic Systems, Measurement and Control*, Vol. 104 No. 1, pp. 65-77.

Appendix

Computation of the contact points

Without loss of generality, we assume that $P_l(x_p - d, y_p, z_p)$ is a point on the side surface of the left peg and that $P_r(x_p + d, y_p, z_p)$ is a point on the side surface of the right peg in the *P*-frame, where d is the distance from the center of the peg to O_p. $(\theta_{pz}, \theta_{py}, \theta_{pz})$ are the angles between the z_p-axis and the three coordinate axes of the *H*-frame. Hence, we can obtain the new expressions of P_l and P_r in the *H*-frame.

Denote the new coordinates of point P_l in the *H*-frame by $(x'_{pl}, y'_{pl}, z'_{pl})$, which are given by:

$$x'_{pl} = x_p \cdot c\theta_{py}c\theta_{pz} + y_p \cdot (s\theta_{px}s\theta_{py}c\theta_{pz} - c\theta_{px}s\theta_{pz}) + z_p \cdot (c\theta_{px}s\theta_{py}c\theta_{pz} + s\theta_{px}s\theta_{pz}) + x_0 \quad \text{(A1)}$$

$$y'_{pl} = x_p \cdot c\theta_y s\theta_z + y_p \cdot (s\theta_{px}s\theta_{py}s\theta_{pz} + c\theta_{px}c\theta_{pz}) + z_p \cdot (c\theta_{px}s\theta_{py}s\theta_{pz} - s\theta_{px}c\theta_{pz}) + y_0 \quad \text{(A2)}$$

$$z'_{pl} = -x_p \cdot s\theta_{py} + y_p \cdot s\theta_{px}c\theta_{py} + z_p \cdot c\theta_{px}c\theta_{py} + z_0 \quad \text{(A3)}$$

where $c\theta$ is $\cos\theta$ and $s\theta$ is $\sin\theta$, (x_0, y_0, z_0) is the position of the origin of the *P*-frame, i.e. O_p, in the *H*-frame.

In addition, a point (x_h, y_h) on the edge of the left hole should satisfy the conditions:

$$(x_h - d)^2 + y_h{}^2 = R_h{}^2, z_h = 0 \quad \text{(A4)}$$

A point (x_p, y_p) on the edge of the end surface and the side surface of the left peg satisfies the conditions:

$$(x_p - d)^2 + y_p{}^2 = R_p{}^2, z_p \in [0, h] \quad \text{(A5)}$$

When contact points exist between the left peg and the left hole, we can obtain the following from equations (A1)-(A5):

$$[a_x x_p + b_x y_p + c_x z_p + x_0 - d]^2 + [a_y x_p + b_y y_p + c_y z_p + y_0]^2 = R_h{}^2 \quad \text{(A6)}$$

$$-a_z \cdot x_p + b_z \cdot y_p + c_z \cdot z_p + z_0 = 0 \quad \text{(A7)}$$

$$(x_p - d)^2 + y_p{}^2 = R_p{}^2 \quad \text{(A8)}$$

$$z_p \in [0, h] \quad \text{(A9)}$$

where:

$$a_x = c\theta_{py}c\theta_{pz}, b_x = s\theta_{px}s\theta_{py}c\theta_{pz} - c\theta_{px}s\theta_{pz},$$
$$c_x = c\theta_{px}s\theta_{py}c\theta_{pz} + s\theta_{px}s\theta_{pz},$$

$$a_y = c\theta_y s\theta_z, b_y = s\theta_{px}s\theta_{py}s\theta_{pz} + c\theta_{px}c\theta_{pz},$$
$$c_y = c\theta_{px}s\theta_{py}s\theta_{pz} - s\theta_{px}c\theta_{pz}$$

$$a_z = -s\theta_{py}, b_z = s\theta_{px}c\theta_{py}, c_z = c\theta_{px}c\theta_{py}$$

We can solve equations (7)-(10) to obtain the contact points between the dual pegs and dual holes. Similarly, we can obtain the contact points between the right peg and the right hole.

Decomposition of the attractive region

Set $\theta_x = \theta_x^*$, $\theta_y = \theta_y^*$, $\theta_z = \theta_z^*$, where θ_x^*, θ_y^*, θ_z^* is treated as a constant vector. The minimum of $g(x, y, \theta_x^*, \theta_y^*, \theta_z^*)$ is denoted by $g(x^*, y^*, \theta_x^*, \theta_y^*, \theta_z^*)$, as expressed in equation (2):

$$g(x^*, y^*, \theta_x^*, \theta_y^*, \theta_z^*) = \min_{x,y \in U_1} g(x, y, \theta_x^*, \theta_y^*, \theta_z^*) \tag{A10}$$

Assume that $D_{TT}g(\theta_x^*, \theta_y^*, \theta_z^*) > 0$, where $T = (x, y)$, D_{TT} denotes the second-order partial derivative with respect to x, y. Thus, the solution to the minima of function $g(x, y, \theta_x^*, \theta_y^*, \theta_z^*)$, (x, y), can be computed from equation (3):

$$D_T g(x, y, \theta_x, \theta_y, \theta_z) = 0 \tag{A11}$$

where D_T is the first partial derivative with respect to $T = (x, y)$.

If $D_{Tg}(x, y, \theta_x^*, \theta_y^*, \theta_z^*)$ is continuous, then there exists an open set U_1 containing (x^*, y^*), an open set U_2 containing $(\theta_x^*, \theta_y^*, \theta_z^*)$, and a differentiable mapping:

$$f : (\theta_x^*, \theta_y^*, \theta_z^*) \to (x^*, y^*) \tag{A12}$$

Therefore, equation (4) can be expressed as:

$$g(f(\theta_x^*, \theta_y^*, \theta_z^*), \theta_x^*, \theta_y^*, \theta_z^*) = \min_{x,y \in U_1} g(x, y, \theta_x^*, \theta_y^*, \theta_z^*) \tag{A13}$$

Let:

$$g_{1,i}(x, y) = g(x, y, \theta_x^i, \theta_y^i, \theta_z^i) \tag{A14}$$

$$g_2(\theta_x, \theta_y, \theta_z) = g(f(\theta_x, \theta_y, \theta_z), \theta_x, \theta_y, \theta_z) \tag{A15}$$

Thus, the function $g(X)$ is converted into a set of sub-functions, $g_{1,i}$ and g_2.

Similarly, the sub-functions g_2 still can be converted a set of sub-functions $g_{2,j}$ and a sub-function g_3, as follows:

$$g_{2,j}(\theta_x, \theta_y) = g(x^{\arg}, y^{\arg}, \theta_x, \theta_y, \theta_z^j) \tag{A16}$$

$$g_3(\theta_z) = g(x^{\arg}, y^{\arg}, \theta_x^{\arg}, \theta_y^{\arg}, \theta_z) \tag{A17}$$

where:

Figure A1 Illustration of the construction of the attractive function with its sub-functions

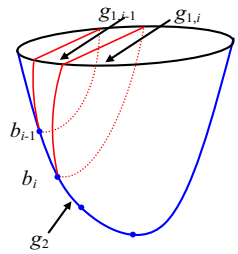

$$(x^{\arg}, y^{\arg}) = \arg \min_{x,y \in U_1} g_{1,i}(x, y) = \arg \min_{x,y \in U_1} g(x, y, \theta_x^i, \theta_y^i, \theta_z^i) \tag{A18}$$

$$(\theta_x^{\arg}, \theta_y^{\arg}) = \arg \min_{\theta_x, \theta_y \in U_2} g_{2,i}(\theta_x, \theta_y) = \arg \min_{\theta_x, \theta_y \in U_2} g(x^{\arg}, y^{\arg}, \theta_x, \theta_y, \theta_z^j) \tag{A19}$$

We can claim that the set of sub-functions are also attractive regions, as:

Theorem a1: All its sub-functions $g_{1,i}$ and g_2 are attractive functions, if the function g is an attractive function.

Proof: Following we will prove that g_2 satisfies the conditions (C1-C3):

- $g_2(R) = g_2(R_0)$ when $R = R_0$ and $g_2(R) > g_2(R_0)$ when $R \neq R_0$ are obvious due to $g(X)$ is a deterministic function.
- Obviously, g_2 has continuous partial derivatives with respect to $(\theta_x, \theta_y, \theta_z)$.
- From:

$$\frac{dg(T, R)}{dt} < 0 \quad \text{in} \quad \Omega - \{T_0, R_0\} \tag{A20}$$

$$\frac{dg_2}{dt} = \frac{d\left(\min_{T \in U_1} g(T, R^*)\right)}{dt} = \frac{\min_{T \in U_1} d(g(T, R^*))}{dt} < 0 \tag{A21}$$

We know that:
Therefore, $dg_2/dt < 0$ in $U_2 - \{R_0\}$.

As g_2 satisfies conditions (C1)-(C3), it is an attractive function in U_2. Similarly, we can prove that $g_{1,i}$ is an attractive function in U_1.

Remark: We use a simple three-dimensional graph to explain the construction of the high-dimensional attractive region with its low-dimensional sub-functions. In Figure A1, $g_{1,i}$ and $g_{1,i-1}$ are two cut profiles on the domain. g_2 constitutes of the minimum of $g_{1,i}$ (i = 1,. . ., n). From Theorem a1, we can know that $g_{1,i}$ and g_2 are attractive functions.

Corresponding author

Jianhua Su can be contacted at: jianhua.su@ia.ac.cn